JPSE (Journal of Physical Science and Engineering), Vol. 7, No. 2, 2022, Page 75–85.
DOI: 10.17977/um024v7i22022p075

JPSE
(Journal of Physical Science and Engineering)

http://journal2.um.ac.id/index.php/jpse
EISSN: 2541-2485

Detection of Lahar Flow Direction from Semeru Eruption on 4 December 2021 using Gravity Method

Received
20 July 2022

Revised
06 September 2022

Accepted for Publication
08 September 2022

Published
24 October 2022

A Realita[1,2*], M N Fahmi[1,2], T Prastowo[1,2], and Madlazim[1,2]

1. Physics Department, Faculty of Mathematics and Natural Sciences, Universitas Negeri Surabaya, Jl. Ketintang, Surabaya, 60231, Indonesia.
2. Center for Earth Science Studies, Faculty of Mathematics and Natural Sciences, Universitas Negeri Surabaya, Jl. Ketintang, Surabaya, 60231, Indonesia.

***E-mail:** arierealita@unesa.ac.id

Abstract
Mount Semeru, an active, steep-sided volcano in East Java, erupted on 4 December 2021 following extreme rainfall that led to an avalanche of hot pyroclastic flows and lahars. Besides a debatable eruption source with no preceding seismic signals observed, it has drawn the international community's attention for its extent of largely impacted areas down the summit. In this study, we used gravity method modeling of the local anomaly in density distribution after the event to determine the unique pattern of the lahar flow direction with the corresponding extent and the spread of the flow. The data were collected from a TOPEX satellite altimeter and processed using a number of specific techniques to obtain a contoured map of local anomaly. The results showed that the main path of the flow was found to descend down the slope to the southeast of the crater, extending to a distance of about 20 km with a maximum lahar flow width of about 2 km toward agricultural lands and populated areas, consistent with the high-resolution satellite imagery produced by UNOSAT-UNITAR. It suggests that gravity anomaly could be used to simulate the flow pattern and the widespread damage of volcanic materials after an eruption.
Keywords: Mount Semeru, pyroclastic flows**,** gravity method, local anomaly.

1. Introduction

Mount Semeru is one of the most active volcanos in a densely populated Java Island, Indonesia. It is primarily bordered by Lumajang and Malang Districts, East Java Province, with its center at 8.1° S and 112.9° E on which its summit reaches 3676 m above sea level [1], [2]. Geologically, the volcano is part of the southern mountain belt in the island, stretching from the west to the east as a consequence of a continually tectonic stress accumulated from the subducting Indo-Australian oceanic crust beneath the Eurasian continental plate [3], [4]. Despite its persistent eruption at varying scales with vast amounts of volcanic materials released and corresponding impacts on the surroundings recorded from past to present times [3], [5], [6], recent research on Semeru is rare owing to the complexity of eruptive behaviors that are difficult to predict and even sometimes with no fatalities reported. However, intense rainfalls on 4 December 2021 triggered a lava dome at the crater being collapsed [7], [8]. In turn, the collapsed dome produced pyroclastic flows of hot ash and lava avalanches, accelerating down an inclined slope, and bringing sedimentary lahar deposits collected from past events around the top into affected areas nearby, causing significant losses of lives and properties.

Following the 4 December 2021 event, volcanic hazard analysis performed to investigate the cause of the eruption has been an important issue. The analysis is then driven by common sense that a similar phenomenon is possible to occur in the future either at the same location or in other places in the Indonesian territory with no signals detected. As with previous studies [9], [10] investigations may, in particular, be directed into the effort to reduce risk from lava flows and lahar hazards in normal and upnormal (extreme weather) conditions. Successful emergency response to such threats requires a good understanding of eruptive potency and associated risk. It may be achieved by applying either a single or a combined method of geophysical surveys to monitor volcanos, hence better focusing on what is important to do for volcanic hazard risk reduction in Indonesia [11], [12]. The use of gravity anomaly in volcanic studies (e.g. [13]) is common as an eruption corresponds to changes in the density

distribution [14], [15] that are relatively easy to observe. Other applications of the gravity method are also frequently found for the detection of active fault zones and other subsurface structures (e.g. [16]), where in practice, it may be combined with magnetic surveys [17], [18]. Recent work [19] developed a volcanotectonic model, proposing a northward migration of volcanic gravity centers from the southern region of East Java at geological time scales. However, there have been no measurements on the flow extension and spreading of lahars from the latest eruption of Semeru using gravity field surveys or satellite observations.

In this study, we analyze and assess the hazardous eruption of Mount Semeru on 4 December 2021 using gravity anomaly. The density distribution after the eruption with respect to the density background may indicate possible paths of the lahar flow. Thus, this study aims to determine the flow pattern and direction with its corresponding extent and spread measured from the source point. We then compare the results acquired from this study with reported findings from relevant work on high-resolution images derived from post-event, reference satellite observations. The present results may provide insight into effective ways of better resilience and disaster preparedness for lahar hazards in the future.

2. Methods

The methodology used in this study included study area, geological setting of Mount Semeru, detailed procedures for data collection and processing, and relevant instruments used.

2.1. Study Area

East Java Province, at which Mount Semeru is located, is bordered by the Indian Ocean to the south and the Java Sea to the north, while Central Java Province (not shown in Figure 1) is lying on the west and Bali Strait is on the east, separating East Java Province from Bali Island (Figure 1, bottom-left panel). The province extends approximately 400 km long and 200 km wide for the borders, with its population reaches about 40 million people, making it the second most populous province in Indonesia [20]. In this study, the coverage area was limited from 8.05° to 8.35° S for latitude positions and 112.75° to 113.15° E for longitude positions (Figure 1, top-right panel).

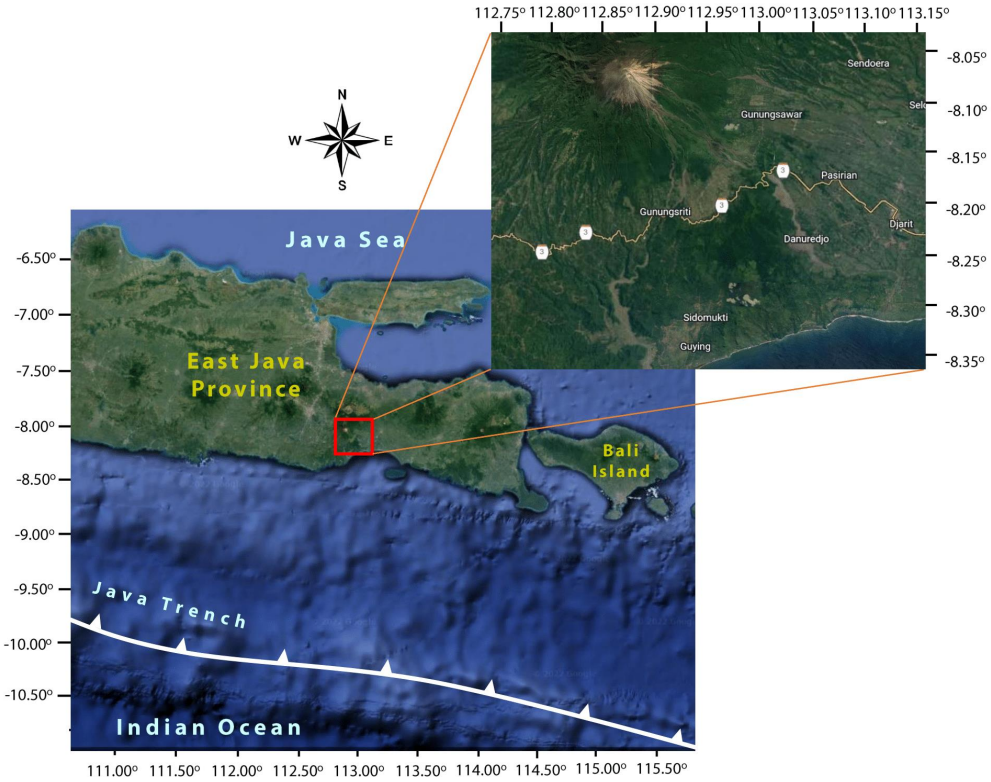

Figure 1. Map showing the location of Mount Semeru in East Java Province (bottom-left panel) with the insert is the volcano seen from an aerial-view observation (top-right panel) where a small part of the Indian Ocean is included (This figure was made available using a Google Earth map and an IRIS website at https://ds.iris.edu/wilber3/find_event).

2.2. Geological Setting

The subsurface geological structure of East Java, the eastern province of Java Island, was formed through highly complicated volcanotectonic activities during the Cenozoic arc magmatism era in the early Tertiary period [21]–[23]. With the southern mountain belt to be the dominant volcanic feature extending along the length of the island, East Java is rich in various mineral deposits, mainly from magmatic processes in the deep, which are extruded near and to the surface during eruptions before becoming sedimentary rocks [1], [3], [24], [25]. Tectonic forces are associated with the presence of the subduction megathrust zone near the Java Trench off the coastline of East Java [4], [12], [26]–[29] and active crustal faults lying on land on the northern side of the province [30]–[32]. Structural changes beneath the surface may also be possible due to geological processes, involving a complex interaction of volcanic and tectonic forces, such as the time evolution of lahar deposits of Semeru [3], [6], [7] and a northward migration of volcanic centers along the Kendeng back-arc thrusting fault [19].

2.3. Data Collection and Processing

The methodology in this study is similar to that discussed in Maghfira *et al*. [13], but with gravity anomaly separation using a filtering technique of upward continuation [33]–[35], applied to secondary data taken from TOPography Experiment (TOPEX) satellite imagery on 10 June 2022. This satellite altimeter is jointly operated by the National Aeronautics and Space Administration (NASA), The US Government Space Agency and Centre National d'Etudes Spatiales (CNES), The French Space Agency, freely accessed at https://topex.ucsd.edu/cgi-bin/get_data.cgi. Two data types were derived from the satellite: gravity field and topography in the study area, as also performed by Setiadi *et al*. [36].

The gravity field data collected from TOPEX was free air anomaly (FAA), including corrections for local gravity effects induced by the elevation measured from the space station to sea surface level (a corrected height), standard for use in oceanic gravity interpretation [13], [36]. The FAA needs to be corrected using Bouguer and terrain corrections. The Bouguer correction revised the average density of rocks between the observer and sea surface level, standard for use in geological interpretation on land. In addition, terrain correction was made available by topographic data and Digital Elevation Model–Shuttle Radar Topography Mission (DEM–SRTM) area in East Java. That was processed by Global Mapper, Excel, and Oasis Montaj, in part the same tool as that used by Dinçer *et al.* [18]. Terrain correction is useful for correcting gravity field data to represent geological settings around the mountain.

The final result of data processing was provided in terms of Complete Bouguer Anomaly (CBA), a map of gravity anomaly made available using Surfer16 with regional and local (residual) anomalies. The (mixed) CBA anomaly was then separated into its components, namely regional and local (residual), using an upward continuation technique [33]–[35], run on MagPick software.

Figure 2 shows a three-dimensional feature of Semeru, drawn using Surfer16. Its appearance is seen from a particular angle of view. The latitudes, longitudes, as well as vertical elevation, are provided for the limitation of the region examined in this study. It is clear that regions of high elevation (light red) around the summit dominate the feature over the surroundings, with the southern region of the volcano close to the coasts toward the Indian Ocean with low elevation (dark blue).

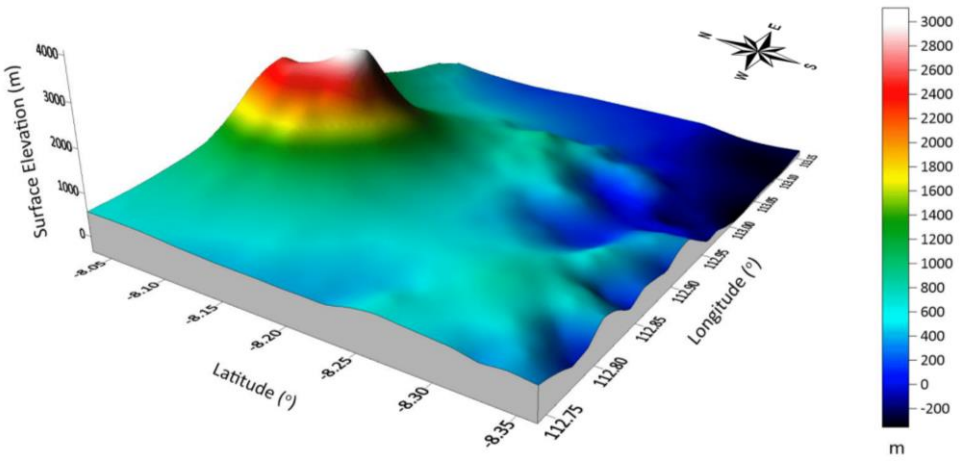

Figure 2. An alternative 3D view of Mount Semeru with its elevation and geographical borders for the study area.

3. Results and Discussions

3.1. Complete Bouguer Anomaly

As detailed in the preceding section, the data collected from TOPEX satellite imagery considering local topography and FAA in the region of interest were corrected using both terrain and Bouguer corrections to derive a CBA gravity model for the study area (Figure 3). As illustrated, a low Bouguer anomaly is marked by blue region with dark blue at its center being a negative Bouguer anomaly around the top, associated with magma fluids concentrated within the magma chamber. Whilst, a relatively high Bouguer anomaly (red horseshoe-shaped area), representing volcanic edifices from past eruptions, is found to surround the crater, in good agreement with recent work [19]. The widespread contours of high densities (red areas) observed in regions of the S and SE direction from the summit show good consistency with earlier reports by [2], [3], [25], indicating the main locations of lahar deposits after the eruptions.

However, the CBA remains challenging to interpret as it consists of mixed gravity anomalies, namely regional anomaly and local anomaly. Here, the local (residual) anomaly is defined as the density contrasts caused by shallow sources near the surface with short wavelengths relative to the background densities, similar to previous work [14], [36]. In the absence of density contrasts, there will be no local anomaly. In some studies [33]–[35], this local anomaly is termed residual anomaly. In contrast, the regional anomaly is related to sources of long wavelengths that serve as noises in this gravity model [14], [36]. Therefore, in this study, we need to separate local anomaly from its corresponding counterpart, regional anomaly, for data enhancement of practical significance using an upward continuation technique [33]–[35].

3.2. Separate Regional and Local Anomalies

The CBA was decomposed into regional and local (residual) components to analyze different contours of density anomaly distributed over the study area under investigation and interpret the results easily. Several separation techniques of gravity anomaly with their own characteristics in details are available in theory (but are not provided here), making the method of anomaly separation is non-unique and hence no single solution is present [37]. For example, an upward continuation technique requires the choice of continuation heights from one level of surface to another level of surface at different altitudes [38], [39]. In this study, the upward continuation (completely performed up to a height of 1000 m) was chosen to be the appropriate technique to better map shallow sources of short-wavelengths in the study area, confirmed by direct comparison between maps of regional and local (residual) anomalies, as shown in Figure 4.

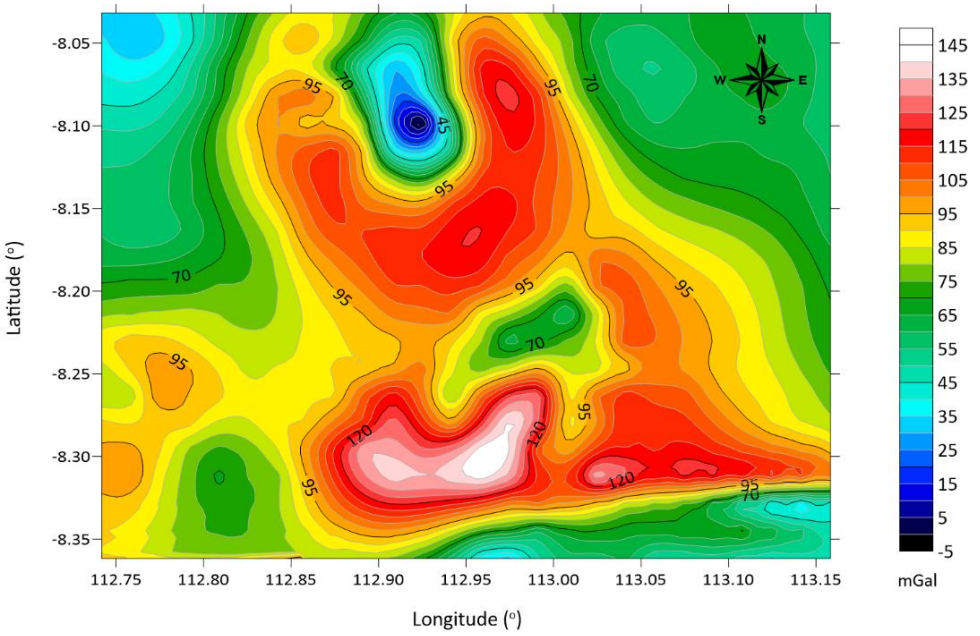

Figure 3. A map of Complete Bouguer Anomaly (CBA) modeled using the gravity method for this study. Contours are made using an interval of 5 mGal for each. Blue and red contours mark areas of low and high anomalies, respectively.

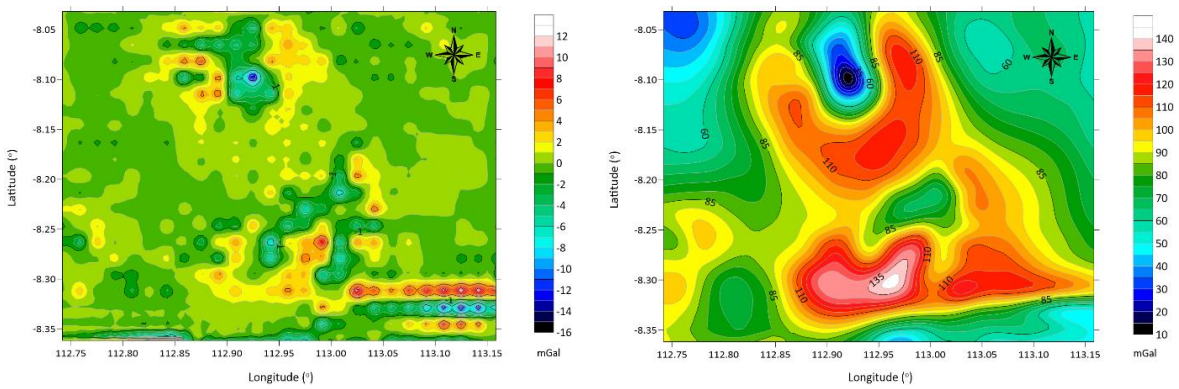

Figure 4. Maps of (a) regional anomaly and (b) local (residual) anomaly, after gravity anomaly decomposition.

There exists a contrast difference in the pattern between regional anomaly (Figure 4a), which is dominated by regions of low Bouguer anomaly (green colors), and local (residual) anomaly (Figure 4b), which is largely covered by a region of high Bouguer anomaly (red colors) with relatively low anomaly found in a small portion only and is surrounded by the red horseshoe-shaped region of high anomaly. The low anomaly feature (ranging from -16 to 12 mGal) for regional anomaly broadly corresponds to magma fluids of relatively low density within the chamber in the deep, compared to other igneous rocks. In this context, regional anomaly is considered to be noises for mapping lahar flow. Whereas, the high anomaly appearance (ranging from 10 to 140 mGal) for local (residual) anomaly represents volcanic edifices or the likely possible lahar deposits from the 4 December 2021 eruption of Mount Semeru.

It is clear that the local (residual) anomaly in Figure 4b is self-similar to the CBA in Figure 3, suggesting this anomaly to be a good choice for mapping the flow pattern (direction and measures) and the density distribution after the event. However, this local (residual) anomaly in its original form cannot be directly used to determine the flow's extent and spread. It requires further processing using a digitizing technique to interpret better the results given in the following section.

3.3. Digitized Local Anomaly for Best Interpretation

For specific purposes, one of which is to determine the flow characteristics examined (flow extent from the source point, which is the summit of Semeru, and flow spreading, to be a maximum width of the dense current downstream), a further process and hence analysis of the local (residual) anomaly for the study area is performed using a digitizing technique. In this context, we provide a line of AA' representing the former and another line of BB' indicating the latter (Figure 5).

For the best interpretation, closures with blue colors having low anomaly, as shown in Figure 5, are associated with the crater in which it is filled with magma fluids of high viscosity but low density, a similar feature to the one discussed in [14] for Mount Pandan, Madiun, East Java. During the event, the flow of dense current (lahar) accelerated downstream in line with the AA' path in the SE direction, reaching a distance of approximately 20 km away from the top in the same manner as reported by previous work [3]. The dense gravity current was actually induced by extreme rainfalls days before and on 4 December 2021, causing the collapse of the volcano dome. In turn, this generated pyroclastic flows and eroded lahar deposits, running down from their concentration around the crater from past eruptions. On its way toward agricultural and plantation lands as well as nearby villages, the dense current advanced with a maximum flow width, seen as BB' in Figure 5, predicted to be about 2 km, bringing all volcanic materials with it to destroy surrounding populated areas. Readers may also refer to earlier studies [1]–[3], [5], [6], [10] for examining lahar deposition processes and corresponding lahar flow hazards, particularly for Mount Semeru. A bank of high-density mass of lahar deposits is also observed in the southern area measured from the summit bordered from -8.25° to -8.35° S and from 112.85° to 113° E. It is just toward the east from this bank. Another lahar deposit of high density is seen between 113° and 113.15° E with the same bordering latitudes. This deposit may be associated with solidifying processes of igneous rocks with higher densities but is not directly related to the eruptive event on 4 December 2021.

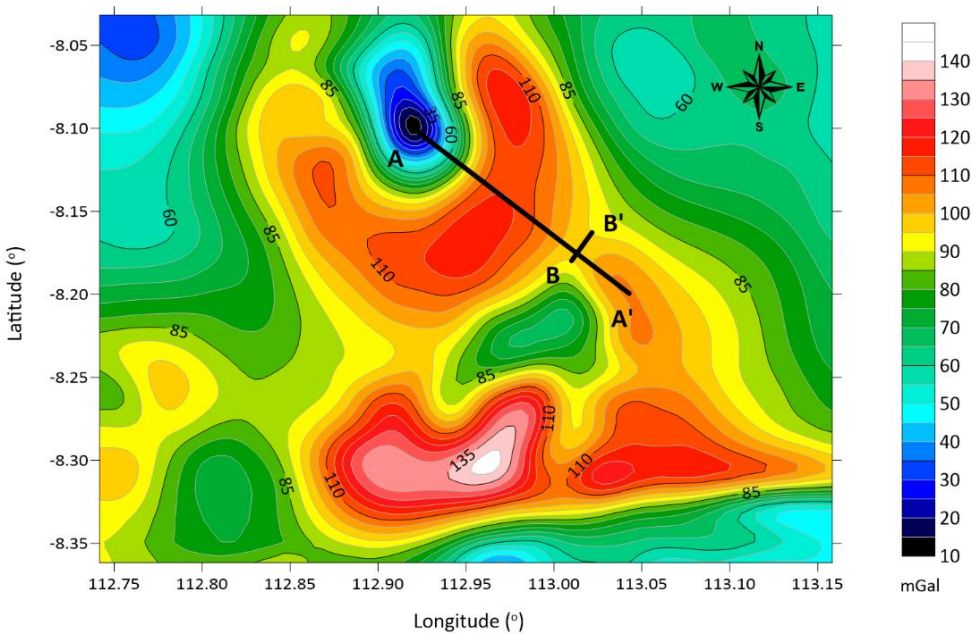

Figure 5. A map of local (residual) anomaly used to determine the extent and the spread of the flow after the Semeru's eruption investigated in this study. Contours are made using an interval of 5 mGal for each. Blue and red contours denote regions of relatively low- and high-density masses, corresponding to low and high anomalies, respectively.

For a better description of lahar deposit movement accelerating along the slope, we combined the 3D view of the topographical features of Mount Semeru (Figure 2) with the resulting contoured map of the local (residual) gravity anomaly (Figure 4b) using an overlay technique, as shown in Figure 6. It is clear from Figure 6 that the high-density mass of lahar deposits is observed, flowing down from regions around the crater to affected areas nearby between 113.05° and 113.15°, which correspond to SE direction with respect to the source (the blue region on the top), in good agreement with previous work on lahar hazards of Mount Semeru [3]. The two banks of lahar deposits, one positioned to the south and the other located to the east from the first bank, are also clearly detected. As earlier mentioned, these deposits may result from cooled extrusive rocks during past eruptions but are not related to the recent event under consideration in this study.

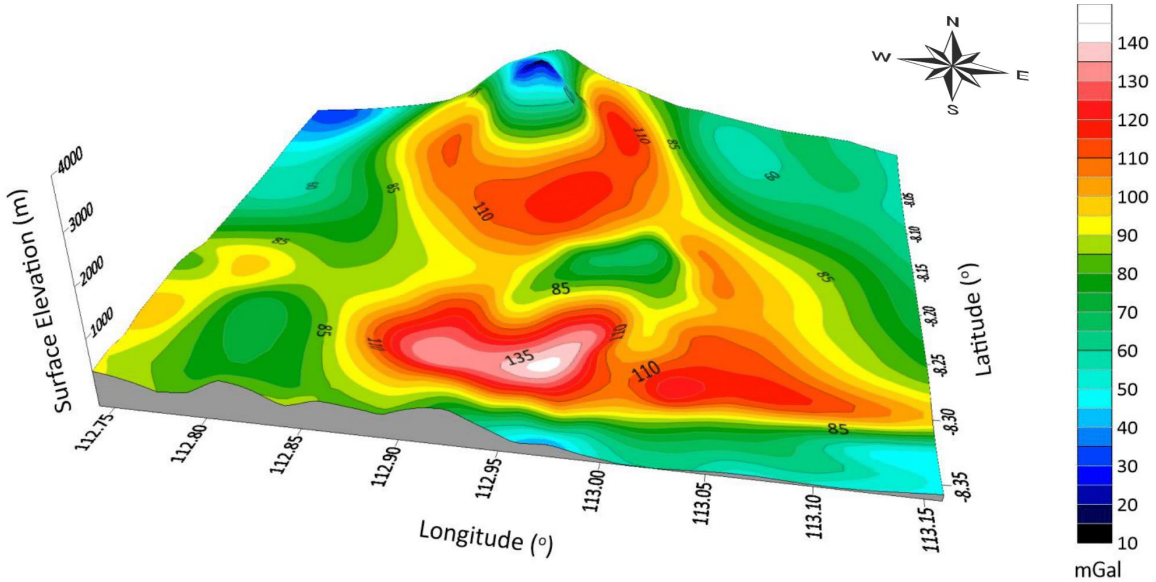

Figure 6. A 3D topographical map of the local (residual) anomaly used to determine the lahar flow pattern and direction after the Semeru's eruption on 4 December 2021 investigated in this study. Contours are made using an interval of 5 mGal for each, where blue and red contours denote regions of relatively low- and high-density deposit masses, corresponding to low- and high-density anomalies, respectively, with respect to the surrounding densities.

In addition to all descriptions above, we bring the gravity anomaly ranging from 10–140 mGal, as illustrated in Figure 6, into attention. Regarding the similarity in color between a 3D topographical map and gravity anomaly scales, we conclude that eroded lahar deposits from the event on 4 December 2021 are composed of volcanic rocks with positive anomalies between 120–125 mGal. This finding is consistent with the Bouguer anomaly map of East Java, where the sub-surface geological structure beneath Semeru was estimated at a value of 0,125 mGal (after simple calculations using the definition of Gal in the unit and corresponding conversion from the standard international (SI) measure to gravity anomaly measured in mGal) [22]. It is easily understood from the theoretical point of view that lahar deposits (extrusive rocks) and molten magma (intrusive rocks) have similar gravity anomaly values. Indeed, this finding fits into a suitable proof of consistency between the resulting gravity modeling performed in this study and that reported in previous work [22].

For comparison, we here provide some aerial photos from satellite-based damage assessment in affected areas on 7 and 11 December 2021 around the crater of Mount Semeru and its surroundings, accessed at https://disasterscharter.org/documents/10180/10749506/vap-850-11-product. These photos are made available by the United Nations Satellite Centre (UNOSAT), managed by the United Nations Institute for Training and Research (UNITAR), where one of its world missions is to provide geospatial data and information for hazard analysis and assessment using satellite technologies. Figure 7 illustrates two conditions around the summit viewed from the satellite on 25 November and 7 December 2021.

The extent to which hot ash and lahar flow deposits affects surrounding areas, including houses, agricultural and plantation lands, and other structures, all the way down from the top, is influenced by some factors. Noted here are counted days after the event. For example, the lahar flow track was observed to extend to a region of 15.5 km away from the source point on 7 December 2021 (Figure 7, right panel). However, it was then extended by the time to reach Sumberwuluh, a small village in the Lumajang District in the southeast direction, with respect to the crater on 11 December 2021. The satellite visually reported the lahar flow to destroy the Sumberwuluh-Candipuro bridge, located about 16.5 km from the source point (Figure 8). However, the flow could be extended several kilometers to a greater distance from the bridge (not seen in Figure 8).

It follows that the flow propagates southeastward over a distance of approximately 20 km or even more, within the range of 20–25 km estimated for the travel distance of rain-induced lahars flowing through the southeast valley each year, as reported by previous work [3]. The results of the present study confirm earlier volcanic studies on lahar threats of Mount Semeru, highlighting how important to understand the geophysical processes of lahar deposit formation [1], to find the likely locations of lahar

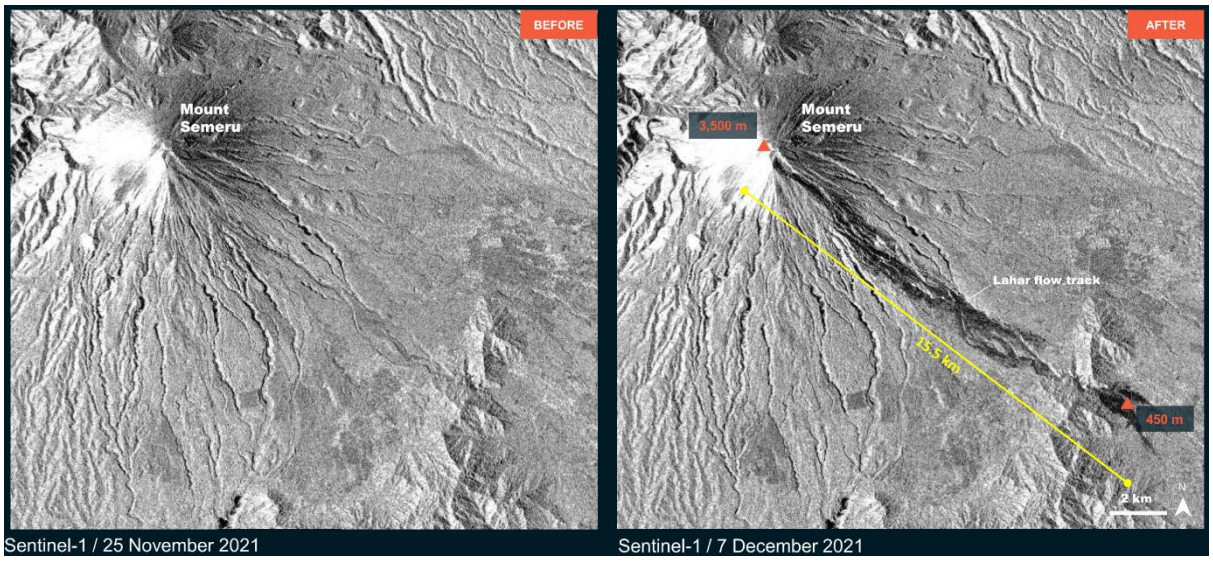

Figure 7. Conditions before and after the 4 December 2021 event observed from satellite imagery provided by UNOSAT-UNITAR. Notice that the yellow straight line with a total length of 15.5 km is measured from the summit (source point) toward a particular location, which is part of the impacted regions downstream Mount Semeru on 7 December 2021 (adopted from https://disasterscharter.org/documents/10180/10749506/vap-850-11-product).

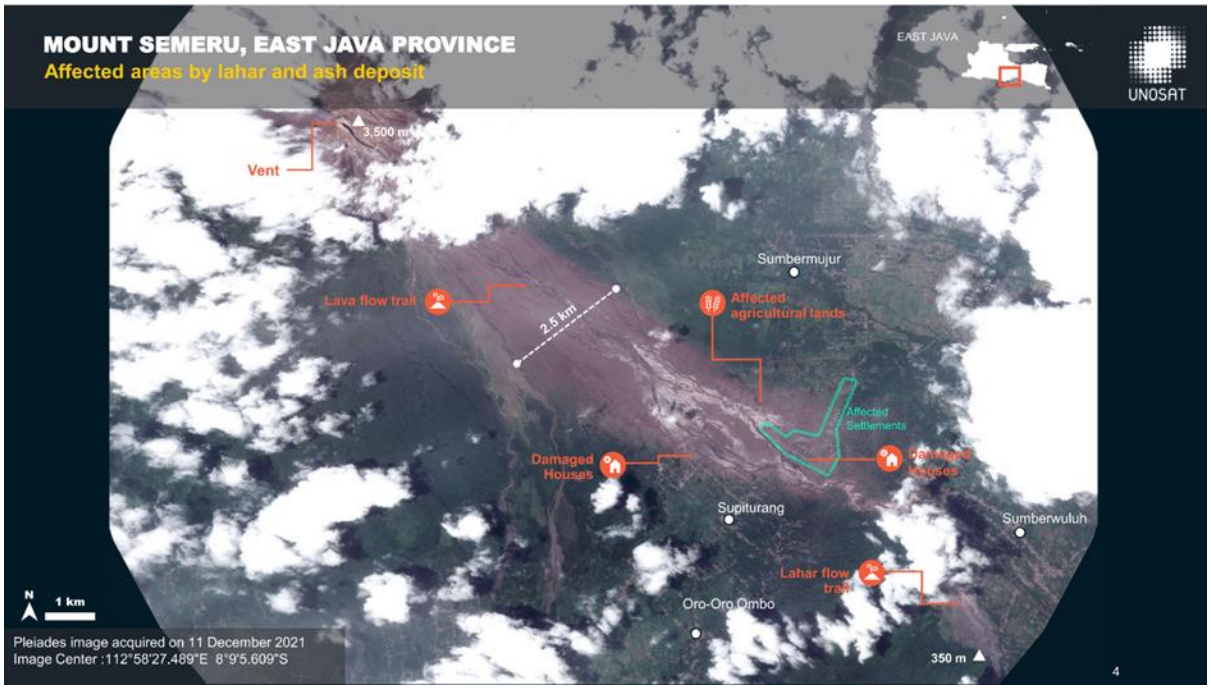

Figure 8. Conditions in widespread lahar-impacted areas on 11 December 2021 observed from satellite imagery provided by UNOSAT-UNITAR (adopted from https://disasterscharter.org/documents/10180/10749506/vap-850-11-product).

hazard-prone areas [3], and to evaluate flow evolution of lahar deposits [6]. These are all dedicated to reducing risk from lahar hazards, as prompted by [10]. However, the caveat of this study is that the present results and the corresponding reference imagery are derived from satellite observations. Thus, future work on possible similar volcanic disasters in Indonesia may work with geophysical field surveys [3] or numerical modeling [1] to complete the observations. In particular, Mount Semeru is proved to be hazardous for local people living nearby owing to the combination of persistent volcanic activity within the magma chamber and possible lahar threats during rainy seasons.

4. Conclusions

The gravity anomaly method has been used to determine the lahar flow pattern and direction, including the extent and the spread of the flow observed from the unique 4 December 2021 Mount Semeru event. The eruption was caused by the extreme rainfall a few days earlier. On the day the event occurred, it triggered the dome's collapse and led to pyroclastic flows of hot lava and dense lahar deposits running downstream from their accumulation around the top from past eruptions. The data from TOPEX are processed as CBA, consisting of mixed anomalies. In turn, these anomalies are further processed and decomposed into separate regional and local anomalies. From the local gravity anomaly mapping, we analyze the flow characteristics of lahars and find that the flow of lahars descends downstream in the southeast direction, extending to a distance of approximately 20 km toward impacted areas with the maximum width of about 2 km. The present results show that the gravity method can be used to monitor volcanic activity. In this context, the method can also be combined with other measures of geophysical techniques to reduce volcanic risk in Indonesia for future work.

Acknowledgments

The authors would like to thank the National Aeronautics and Space Administration (NASA), The US Government Space Agency dan Centre National d'Etudes Spatiales (CNES), and The French Space Agency for the data used in this study available from a Topography Experiment (TOPEX) satellite provided at https://topex.ucsd.edu/cgi-bin/get_data.cgi by The Scripps Institution of Oceanography, The University of California at San Diego (UCSD), US. This study is made possible by Universitas Negeri Surabaya through funding available under a research grant scheme of Penelitian Kebijakan Fakultas Tahun 2022 No. B/36605 /UN38.3/LK.04.00/2022.

References

[1] C. Gomez, F. Lavigne, D. S. Hadmoko, and P. Wassmer, "Insights into lahar deposition processes in the Curah Lengkong (Semeru Volcano, Indonesia) using photogrammetry-based geospatial analysis, near-surface geophysics and CFD modelling," *J. Volcanol. Geotherm. Res*., vol. 353, pp. 102–113, 2018, doi: 10.1016/j.jvolgeores.2018.01.021.

[2] A. Loeqman *et al.*, *Gunung Api Indonesia dan Karakteristik Bahayanya*. Bandung, Indonesia: Pusat Vulkanologi dan Mitigasi Bencana Geologi, 2020.

[3] J. C. Thouret, F. Lavigne, H. Suwa, B. Sukatja, and Surono, "Volcanic hazards at Mount Semeru, East Java (Indonesia), with emphasis on lahars," *Bull. Volcanol.*, vol. 70, no. 2, pp. 221–244, 2007, doi: 10.1007/s00445-007-0133-6.

[4] Fahrudin, A. S. Hidayatullah, and M. J. Maulana, "Tectonic relationships and structural development between Arjosari, Pacitan, East Java and Tawangmangu, Karanganyar, Central Java," in *The 1st Int. Conf. Geodesy Geomat. Land Adm. 2019*, pp. 47–56, 2019, doi: 10.18502/keg. V 4i3.5822.

[5] A. Solikhin, J. C. Thouret, A. Gupta, A. J. L. Harris, and S. C. Liew, "Geology, tectonics, and the 2002–2003 eruption of the Semeru volcano, Indonesia: interpreted from high-spatial resolution satellite imagery," *Geomorphology*, vol. 138, no. 1, pp. 364–379, 2012, doi: 10.1016/j.geomorph.2011.10.001.

[6] C. C. A. Starheim, C. Gomez, T. Davies, F. Lavigne, and P. Wassmer, "In-flow evolution of lahar deposits from video-imagery with implications for post-event deposit interpretation, Mount Semeru, Indonesia," *J. Volcanol. Geotherm. Res*., vol. 256, pp. 96–104, 2013, doi: 10.1016/j.jvolgeores.2013.02.013.

[7] Wikipedia. "2021 Semeru eruption." en.wikipedia.org. https://en.wikipedia.org/wiki/2021_Semeru_eruption (accessed July 13, 2022).

[8] The United Nations Office for the Coordination of Humanitarian Affairs (OCHA). "Indonesia: Semeru Volcano - Dec 2021." reliefweb.int. https://reliefweb.int/disaster/vo-2021-000194-idn (accessed July 13, 2022).

[9] L. J. Connor, C. B. Connor, K. Meliksetian, and I. Savov, "Probabilistic approach to modeling lava flow inundation: a lava flow hazard assessment for a nuclear facility in Armenia," *J. Appl. Volcanol.*, vol. 1, no. 3, pp. 1–19, 2012, doi: 10.1186/2191-5040-1-3.

[10] T. C. Pierson, N. J. Wood, and C. L. Driedger, "Reducing risk from lahar hazards: concepts, case, studies, and roles for scientists," *J. Appl. Volcanol.*, vol. 3, no. 16, pp. 1–25, 2014, doi: 10.1186/s13617-014-0016-4.

[11] A. Simpson, R. W. Johnson, and P. Cummins, "Volcanic threat in developing countries of the Asia–Pacific region: probabilistic hazard assessment, population risks, and information gaps," *Nat. Hazards*, vol. 57, pp. 151–165, 2011, doi: 10.1007/s11069-010-9601-y.

[12] P. R. Cummins, "Geohazards in Indonesia: Earth science for disaster risk reduction–introduction," *Geol. Soc. Spec. Publ*., vol. 441, pp. 1–7, 2017, doi: 10.1144/SP441.

[13] P. Maghfira and S. Niasari, "Gravity satellite data analysis for subsurface modelling in Mount Merapi-Merbabu, Java, Indonesia," *E3S Web Conf.*, vol. 76, p. 03003, 2019, doi: 10.1051/e3sconf/20197603003.

[14] D. Santoso *et al.*, "Gravity structure around Mt. Pandan, Madiun, East Java, Indonesia and its relationship to 2016 seismic activity," *Open Geosci*., vol. 10, no. 1, pp. 882–888, 2018, doi: 10.1515/geo-2018-0069.

[15] S. Okubo, "Advances in gravity analyses for studying volcanoes and earthquakes," *Proc. Jpn. Acad., Ser. B Phys. Biol. Sci.*, vol. 96, no. 2, pp. 50–69, 2020, doi: 10.2183%2Fpjab.96.005.

[16] Y. Ming *et al.*, "Application of gravity exploration in urban active fault detection," *IOP Conf. Ser. Earth Environ. Sci.*, vol. 660, p. 012057, 2021, doi: 10.1088/1755-1315/660/1/012057.

[17] B. K. Amoah, I. Dadzie, and K. T. Kyeremeh, "Integrating gravity and magnetic field data to delineate structurally controlled gold mineralization in the Sefwi Belt of Ghana," *J. Geophys. Eng.*, vol. 15, no. 4, pp. 1197–1203, 2018, doi: 10.1088/1742-2140/aaa7b2.

[18] B. Dinçer and V. Işik, "Determination of structural characteristics of Tuzgölü Fault Zone using gravity and magnetic methods, Central Anatolia," *Bull. Miner. Res. Explor.*, vol. 162, no. 162, pp. 145–174, 2020, doi: 10.19111/bulletinofmre.661245.

[19] M. Lupi *et al.*, "Northward migration of the Javanese volcanic arc along thrust faults," *Earth Planet. Sci. Lett.*, vol. 577, p. 117258, 2022, doi: 10.1016/j.epsl.2021.117258.
[20] Directorate of Population and Employment Statistics, "Hasil Sensus Penduduk 2020," Indonesian Bureau of Statistic, Jakarta, Indonesia, Berita Resmi Statistik No. 7/01/Th. XXIV, Jan. 2021.
[21] L. D. Setijadji, S. Kajino, A. Imai, and K. Watanabe, "Cenozoic Island arc magmatism in Java Island (Sunda Arc, Indonesia): Clues on relationships between geodynamics of volcanic centers and ore mineralization," *Resour. Geol.*, vol. 56, no. 3, pp. 267–292, 2006, doi: 10.1111/j.1751-3928.2006. tb00284. X.
[22] H. R. Smyth, R. Hall, and G. J. Nichols, "Cenozoic volcanic arc history of East Java, Indonesia: the stratigraphic record of eruptions on an active continental margin," *Geol. Soc. Am. Spec. Pap.*, vol. 436, pp. 199–222, 2008, doi: 10.1130/2008.2436(10).
[23] A. Susilo and Z. Adnan, "Probabilistic seismic hazard analysis of East Java region, Indonesia," *Int. J. Comput. Electr. Eng.*, vol. 5, no. 3, pp. 341–344, 2013, doi: 10.7763/IJCEE. 2013.V5.728.
[24] A. Y. Al-Hakim and B. Sulistijo, "Integrated exploration method to determine Cu prospect in Seweden district, Blitar, East Java," *Proc. Earth Planet. Sci.*, vol. 6, pp. 64–69, 2013, doi: 10.1016/j.proeps.2013.01.009.
[25] A. A. Martha, P. Cummins, E. Saygin, S. Widiyantoro, and Masturyono, "Imaging of upper crustal structure beneath East Java–Bali, Indonesia with ambient noise tomography," *Geosci. Lett.*, vol. 4, no. 1, p. 14, 2017, doi: 10.1186/s40562-017-0080-9.
[26] A. Špičák, V. Hanuš, and J. Vaněk, "Earthquake occurrence along the Java trench in front of the onset of the Wadati-Benioff zone: Beginning of a new subduction cycle?," *Tectonics*, vol. 26, no. 1, pp. 1–16, 2007, doi: 10.1029/2005TC001867.
[27] A. N. Nugraha *et al.*, "Hypocenter relocation along the Sunda Arc in Indonesia, using a 3D seismic-velocity model," *Seismol. Res. Lett.*, vol. 89, no. 2A, pp. 603–612, 2018, doi: 10.1785/0220170107.
[28] S. Widiyantoro *et al.*, "Implications for megathrust earthquakes and tsunamis from seismic gaps south of Java Indonesia," *Sci. Rep.*, vol. 10, p. 15274, 2020, doi: 10.1038/s41598-020-72142-z.
[29] S. J. Hutchings and W. D. Mooney, "The seismicity of Indonesia and tectonic implications," *Geochem. Geophys. Geosyst.*, vol. 22, no. 9, pp. 1–42, 2021, doi: 10.1029/2021GC009812.
[30] N. Nguyen, J. Griffin, A. Cipta, and P. R. Cummins, "Indonesia's historical earthquakes: modelled examples for improving the national hazard map," *Geoscience Australia*, pp. 1–79, 2015, doi: 10.11636/Record.2015.023.
[31] A. Koulali *et al.*, "The kinematics of crustal deformation in Java from GPS observations: implications for fault slip partitioning," *Earth Planet Sci. Lett.*, vol. 458, pp. 69–79, 2017, doi: 10.1002/2016GL067941.
[32] A. Koulali *et al.*, "Crustal strain partitioning and the associated earthquake hazard in the eastern Sunda-Banda Arc," *Geophys. Res. Lett.*, vol. 43, no. 5, pp. 1943–1949, 2016, doi: 10.1002/2016 GL067941.
[33] Ilapadila, B. Harimei, and Maria, "Analysis of regional anomaly on magnetic data using the upward continuation method," *IOP Conf. Ser. Earth Environ. Sci.*, vol. 297, no. 1, p. 012037, 2019, doi: 10.1088/1755-1315/279/1/012037.
[34] H. Kebede, A. Alemu, and S. Fisseha, "Upward continuation and polynomial trend analysis as a gravity data decomposition, case study at Ziway-Shala basin, central Main Ethiopian rift," *Heliyon*, vol. 6, no. 1, p. e03292, 2020, doi: 10.1016/j. heliyon. 2020. e03292.
[35] I. Setiadi, Marjiyono, and T. B. Nainggolan, "Gravity data analysis based on optimum upward continuation filter and 3D inverse modelling (case study at sedimentary basin in volcanic region Malang and its surrounding area, East Java)," *IOP Conf. Ser. Earth Environ. Sci.*, vol. 873, no. 1, p. 012008, 2021, doi: 10.1088/1755-1315/873/1/012008.
[36] I. Setiadi, J. Widodo, and T. B. Nainggolan, "Geological interpretation of offshore Central Sumatra basin using TOPEX satellite gravity data," *IOP Conf. Ser. Earth Environ. Sci.*, vol. 944, no. 1, p. 012034, 2021, doi: 10.1088/1755-1315/944/1/012034.
[37] W. J. Hinze, R. R. B. von Frese, and A. H. Saad, *Gravity and Magnetic Explorations: Principles, Practices, And Applications*. Cambridge, United Kingdom: Cambridge Uni Press, pp. 1–512, 2013, doi: 10.1017/CBO9780511843129.

[38] D. Ravat, "Upward and downward continuation," in *Encyclopedia of Geomagnetism and Paleomagnetism*, D. Gubbins and E. H. Bervera, Eds., Cham, Switzerland: Springer, pp. 974-976, 2007, doi: 10.1007/978-1-4020-4423-6_311.

[39] M. Pilkington and O. Boulanger, "Potential field continuation between arbitrary surfaces–Comparing methods," *Geophys*., vol. 82, no. 3, pp. 9–25, 2017, doi: 10.1190/geo2016-0210.1.